Neuropathology of Mild Traumatic Brain Injury: Relationship to Structural Neuroimaging Findings

8

Erin D. Bigler

Introduction

The limits of neuroimaging technology specify what types of neuropathology can be detected in traumatic brain injury (TBI), especially if the injury is mild. Fortunately, tremendous advances in neuroimaging technologies, especially with magnetic resonance (MR) imaging (MRI), have been made in the last few years, even in detection of subtle pathology following mild TBI (mTBI). Most conventional MR studies configure anatomical images with millimeter resolution, meaning that structural MRI detects pathology at a similar level, although submillimeter resolution is now possible [1, 2]. However, the fundamental pathological changes that occur from mTBI happen at the micron and nanometer cellular level [3]. This means for brain injuries in the mild range, with the subtlest of neural injuries that the macroscopic lesions characteristic of more severe pathologies simply is not visible in most cases. For example, Fig. 8.1 is from Mayer et al. [4] that examined the frequency of visually objective findings in mild TBI in a large multisite sample of mTBI pediatric cases, initially identified and diagnosed in the emergency department but then followed up with MRI. As shown in Fig. 8.1, while visible abnormalities on MRI may be seen in cases of mTBI, they are only detected in a minority of the mTBI cases scanned and tend to be singular findings. Accordingly, there is a low yield in standard, routine clinical neuroimaging in detecting mTBI abnormalities. Fortunately, with contemporary advances in neuroimaging quantification and analysis, these advanced neuroimaging methods have provided improved insights into how underlying neuropathology associated with mTBI and how it can be detected [5, 6].

E. D. Bigler (✉)
Department of Psychology and Neuroscience Center, Brigham Young University, Provo, UT, USA

Departments of Psychiatry and Neurology, University of Utah, Salt Lake City, UT, USA
e-mail: erin_bigler@byu.edu

S. M. Slobounov, W. J. Sebastianelli (eds.), *Concussions in Athletics*,
https://doi.org/10.1007/978-3-030-75564-5_8

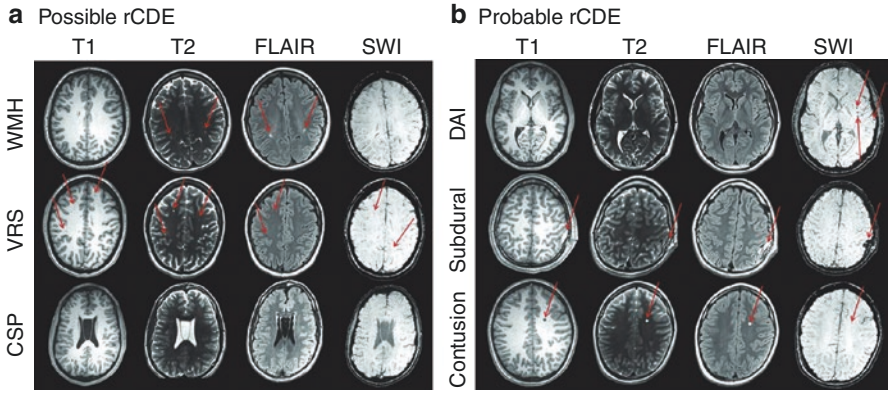

Fig. 8.1 (**a**) Selection of radiologic common data elements, or rCDEs, of possible (a) and probable (**b**) traumatic origin across four different MRI sequences. Cavum septum pellucidum (CSP), hematomas, and contusions were readily visible across T1-weighted, T2-weighted, fluid-attenuated inversion recovery (FLAIR), and susceptibility-weighted imaging (SWI) sequences. White matter hyperintensities (WMH) and prominent perivascular spaces (Virchow-Robin spaces [VRs]) were differentiated by their more conspicuous appearance on FLAIR and T2 sequences, respectively. In contrast, diffuse axonal injuries (DAI) were almost exclusively visible on SWI sequences. Note that abnormalities may only be observed on certain MRI sequences

From review of the images in Fig. 8.1, it is also evident that the location, size, and distribution of MRI abnormalities in mTBI are very heterogeneous. It is also evident that many of these visible abnormalities are small and sometimes rather inconspicuous. This is quite different from what may be observed in moderate-to-severe TBI. Straightforwardly, the contrast in gross visible detection of pathology from mild-to-severe TBI is demonstrated in Fig. 8.2.

In Fig. 8.2, all of the individuals with mTBI had a postresuscitation Glasgow Coma Scale [7] score of 15 and were part of the social outcomes of brain injury in kids [SOBIK] [8] investigation. Although all children in the SOBIK investigation who sustained mTBI had positive day-of-injury (DOI) computed tomography (CT), in the form of contusion, petechial hemorrhage, skull fracture, or edema, only about two-thirds of the 41 mTBI children had identifiable MRI abnormalities when followed up approximately a year or more postinjury. As demonstrated in the Bigler et al.'s [8] investigation, a number of children with subtle hemorrhage and/or localized edema on the DOI CT did not evidence visibly detectable abnormalities on follow-up MRI performed at least a year postinjury. While not possible in human mTBI studies, animal investigations that model mTBI where acute neuroimaging abnormalities become nondetectable over time nonetheless may show residual pathology at the histological level [9–11]. As such, it is safe to assume that DOI pathology like petechial hemorrhages that are not detected on follow-up imaging nonetheless indicates significant shear forces were present in the brain at the time of injury and likely do reflect where residual pathology may be present at the cellular level, just not detectable with contemporary neuroimaging methods.

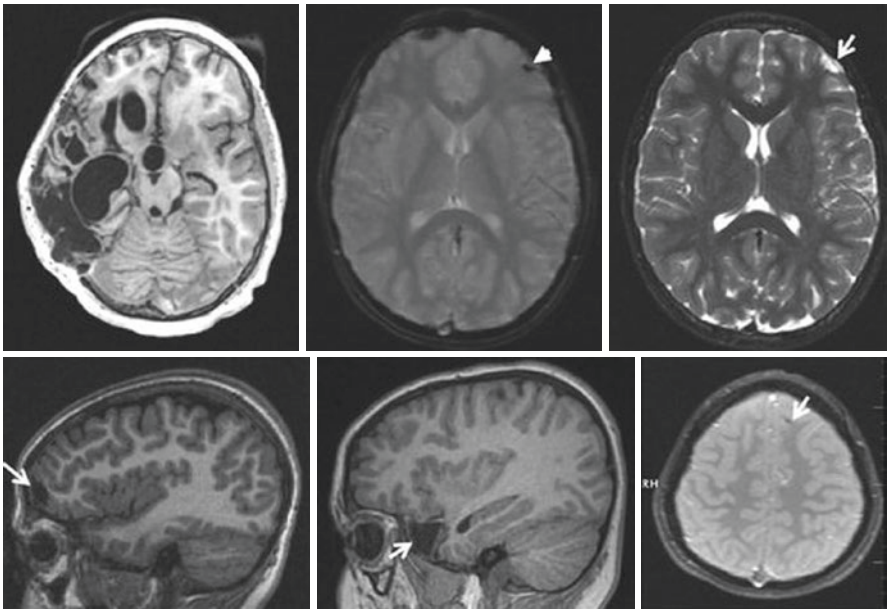

Fig. 8.2 The subtleness and diversity of MRI identified chronic (>6 months postinjury) brain lesions in four mTBI patients, all with a GCS of 15, compared to the massive structural pathologies associated with severe TBI presented in this figure. The mTBI case shown in the *top middle* and *right* shows characteristic area of small focal encephalomalacia with increased region of CSF (*arrow*) in the T2-weighted image (*top right*) associated with residual hemosiderin (*arrowhead*) in the gradient-recalled echo (GRE) sequence (*top middle*). These pathological changes were originally the result of a focal frontal contusion. In the sagittal image in the *bottom left*, focal frontal encephalomalacia is evident (*arrow*) and encephalomalacia in the temporal lobe (*arrow*) in the *middle* image with the *bottom right* image showing an axial scan with subtle hemosiderin right at the gray-white junction (*arrow*), all from different children. In contrast, the child with severe injury (axial view, *upper left*) has massive structural pathology. (From Bigler et al. [8]; used with permission)

The introduction above highlights the "visible" abnormalities in mTBI, but structural neuroimaging also provides other metrics to assess the pathoanatomical nature of injury. When abnormalities are detected, how does this assist the clinician or researcher in understanding outcome and treatment? In the last few years, a variety of both structural and functional neuroimaging techniques have led to a more informed approach for understanding brain networks, along with how network damage/dysfunction accompanies TBI [3, 12]. This is a particularly important neuroimaging and cognitive neuroscience advancement because the inference about location of the lesion or structural abnormality in mTBI may not be the most important factor associated with a traumatic injury, but how that traumatic pathology disrupts network functioning.

Figure 8.3 summarizes some of the network advances since the previous edition of this text [5]. In mathematics, graph theory provides metrics to examine pairwise relations between objects [13]. For brain structure, an "object" is defined as either a

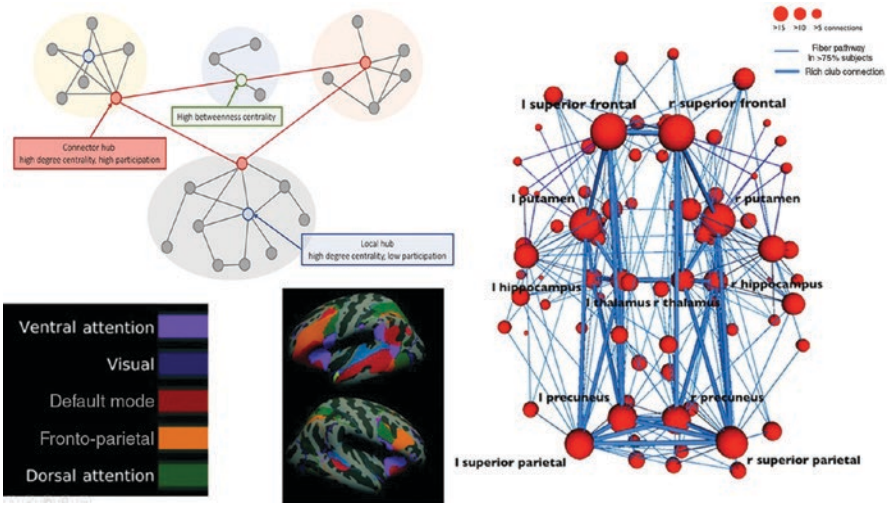

Fig. 8.3 (Top Left) The network schematic is from Arnatkeviciute and Fulcher [13], which shows different concepts of hubness in brain networks. A schematic representation of a modular network where nodes within a module (different background colors) show a relatively high degree of intramodular connectivity and a low degree of intermodular connectivity. High-degree nodes can be classified into (i) local hubs (blue) that have a high-degree centrality and low participation coefficient; and (ii) connector hubs (red) that have high degree and connect to nodes in other modules. Nodes with high betweenness centrality are located on shortest paths between nodes and can play an important role in linking different nodes, even if they have low degree (e.g., the green node supports communication between the yellow and orange modules). (Bottom Left) Adapted with permission from Bailey, Aboud [15] depicts several of the multicortical loci for different networks. Note how the regional representation is never in just one area, indicating the dependence of the network on white matter connectivity. The "Rich Club" network depicted to the right is from van den Heuvel and Sporns [16], used with permission. The schematic depicts the group connectome with rich-club connections marked in dark blue. Connections between rich-club regions (dark blue) and connections from rich-club nodes to the other regions of the brain network (light blue) link via hubs which vary in their strength of connection as reflected in their size. The figure shows that almost all regions of the brain have at least one link directly to the rich club

region of interest (ROI) or at a cellular level, how neuron A connects with neuron B, so on [3]. Connection strength is mathematically determined, where, as shown in Fig. 8.3, a graph matrix is generated by various vertices that connect two points or nodes which are connected by edges, forming linkage between those areas (see upper left, Fig. 8.3). Several important neuroimaging-derived networks are presented in Fig. 8.3 (bottom left). Note that each network has a rather diverse array of cortical representations, where each region of the network needs to be interconnected for a particular domain to function, meaning that connectivity is directly dependent on the health of axon integrity, ergo, and brain white matter. Accordingly, where traumatic pathology of any type may reside, the location of the pathology may not be as important as knowing how a particular network is affected. The importance of this point is that any focal TBI pathology has the potential to distally affect and disrupt the network far from the specific source of the pathology.

The image on the right of Fig. 8.3 provides a schematic of what is referred to as a "Rich Club" network, which euphemistically refers to the most critical parts of the network, including critical central hubs [14]. The importance of the network in this illustration is signified by the width of the connector lines and size of the hub icon. On the periphery of a network, minor connector points or nodes of a network probably have some redundancy with other aspects of the network where either via network adjustment or re-routing minimal to no damage to the network occurs, when that minor node is damaged. In this scenario of reworking the network, over time the effects of the injury may not be functionally detectable. On the other hand, if there is substantial pathology directly affecting a major hub, then more devastating effects occur, or if numerous peripheral nodes within a system get disrupted.

Because of these limitations with neuroimaging resolution in detecting abnormalities, a simple distinction in structural imaging may be developed between lesions or abnormalities visibly identified at the macroscopic level and those more empirically or quantitatively derived from scan metrics. This distinction between visible versus empirically derived quantitative metrics will be further explored in this chapter but first some mention of the role of CT in TBI will be discussed because it is the most common initial or emergently performed structural imaging modality performed in TBI, including mTBI [6, 17–19]. As such, typically, the first neuroimaging findings in TBI are CT based, providing important baseline information even when entirely negative. This chapter will not cover functional neuroimaging or magnetic resonance (MR) spectroscopy (MRS) as these techniques will be covered elsewhere and have previously been reviewed by Slobounov et al. [20]. Also, fundamentals of imaging will not be covered in this chapter as a variety of publications provide such information [21, 22].

Heterogeneity of mTBI

As already alluded to and shown in Figs. 8.1 and 8.2, no two head injuries are identical [23]. Even with the careful precision of animal models no two injuries can ever be identically replicated [24]. If one now adds to the complexity, individual differences in human development and experience (the brain is an experience/age-dependent organ), combined with genetic endowment and whatever unique circumstances that occur with each injury, an incredible mix of events and circumstance accompanies every injury. So, the pathology that is detectable via neuroimaging techniques will never be identical across individuals but there are common pathologies. As will be explained in greater detail throughout this chapter, particular vulnerability of white matter (WM) underlies much of the pathology associated with mTBI. The majority of axons are myelinated; with the vulnerability of WM damage from trauma, the WM designation infers that the axon element of the neuron is particularly susceptible in TBI. Interneuronal connection occurs via axons; thus, WM pathology in TBI may be considered a problem of neural connectivity, disruptive of the WM architecture that makes up neural networks as depicted in Fig. 8.3. With a neuron's cell body densely compacted within the gray matter

neuropil and held tightly within this matrix of cell bodies, the axon extension becomes vulnerable because WM pathways course in multiple directions of various lengths creating a bend and interwoven lattice work of projecting axons. This makes WM especially vulnerable to stretch, strain, and tensile effects following mechanical deformation that occurs with impact injury [17, 18, 25, 26]. This is depicted in Fig. 8.4, which shows that only certain WM tracts are actually damaged within a particular biomechanical strain field (see [27]). Watanabe et al. [28] have shown how with each individual impact injury, unique influences occur from the biomechanical movement of the brain within the cranium in relation to body impact. In

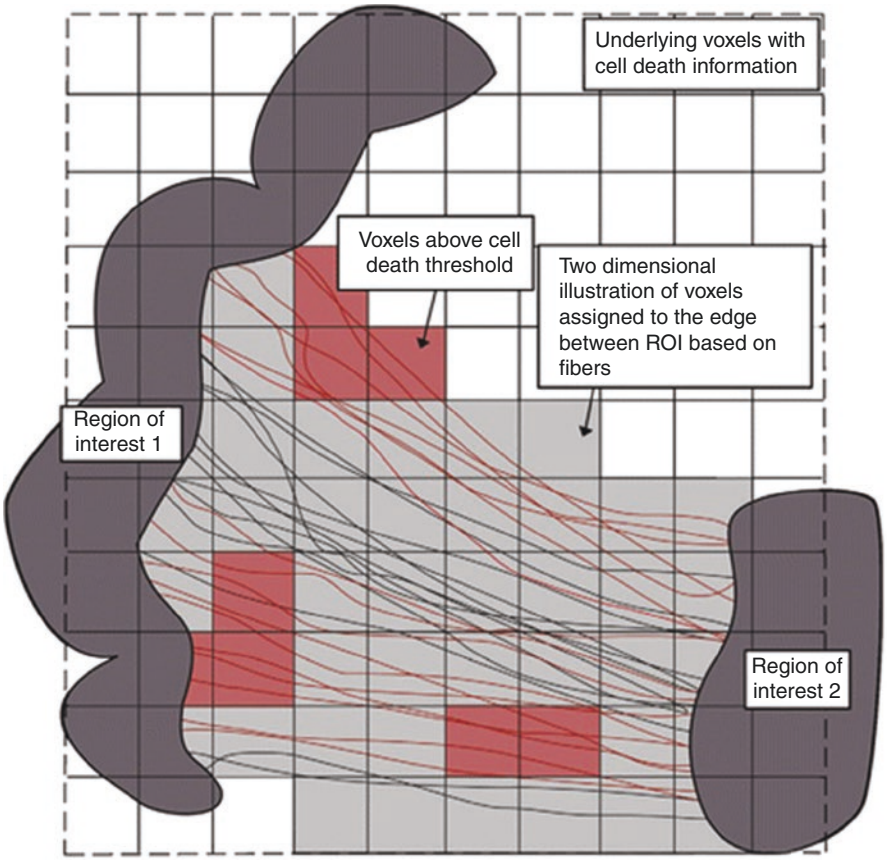

Fig. 8.4 This schematic shows how different axon trajectories may or may not be vulnerable to injury. As can be seen, there are only certain sectors where the biomechanical deformation sufficiently alters brain parenchyma to damage axons. *Lines* represent hypothetical axon projections from one gray matter structure to another. Note that even though all connect region of interest (ROI) 1 with ROI 2, and that out of all sectors where these hypothetical axons project, only eight of the sectors experienced sufficient deformation to damage axons because of the differences in crossing routes and trajectories numerous axons that were affected. (From Kraft et al. [27]; used with permission)

particular, Watanabe et al. show that with basic biomechanical modeling of injury that as the upper brainstem merges into the region of the base of the thalamus and internal capsular area, this also represents the center of parenchymal movement with simple acceleration and rotation. The point to make with this observation, is that some of the greatest strain occurs subcortically. However, the Watanabe et al. simulations also demonstrated that each injury produced unique brain displacement based on individual characteristics of impact biomechanics. These unique individual differences, when coupled with the fact that neural tissue has different elastic properties that are region and structure dependent [25], further reinforces the concept that no two injuries from mTBI will ever produce identical pathology detectable by neuroimaging. More about the biomechanics and regions of vulnerability will be reviewed at the end of the chapter.

Time Sequence of Neuropathology Associated with mTBI

There can be no dispute that an acute brain injury has occurred in a witnessed traumatic event associated with positive loss of consciousness (LOC) and obvious biomechanical forces. Therefore, such cases represent the best model for understanding the time sequence of symptom resolution and return to baseline function. The case shown in Fig. 8.5, which displays a negative DOI CT scan, provides such an example. This young adult female sustained an mTBI in an auto-pedestrian accident. She was struck by a passing car while standing next to her vehicle with family members nearby, but no other family member was struck or injured. She was thrown into the air striking her head on the curb, resulting in immediate LOC (no skull fracture), which lasted 2–3 min according to eyewitness family members present at the time of the accident. Emergency medical services were on the scene within 10 min, where they found her conscious but confused. She had orthopedic injuries to her legs (ligament knee injuries) and was stabilized and transported to the emergency department (ED) with a GCS of 15 noted on intake. During ED observation over the next couple of hours, GCS fluctuated between 13 and 15. With the head DOI CT being negative (see Fig. 8.5; top left), but given the severity of the impact, positive LOC, and fluctuating level of GCS she was monitored overnight and discharged the next day, with outpatient follow-up provided through the hospital concussion care program. Interestingly, her postconcussive symptoms (PCS) of headache, mental confusion, lethargy, and sleepiness increased in the days that followed. Some have speculated that PCS reaches its apex on the DOI and then dissipates. While true for some, peak symptoms following mTBI may occur hours to days postinjury [29, 30], which was the case with this patient. She was a student and attempted to go back to her studies approximately 3 weeks postinjury but experienced major cognitive challenges, especially problems with focused and sustained attention along with fatigue. Because of the persistence in symptoms and that MRI studies had not been done, several weeks postinjury an MRI was obtained which demonstrated residual hemosiderin deposition scattered in the right frontal region as shown in Fig. 8.5, which also corresponded to scattered WM hyperintensities. These abnormalities remained

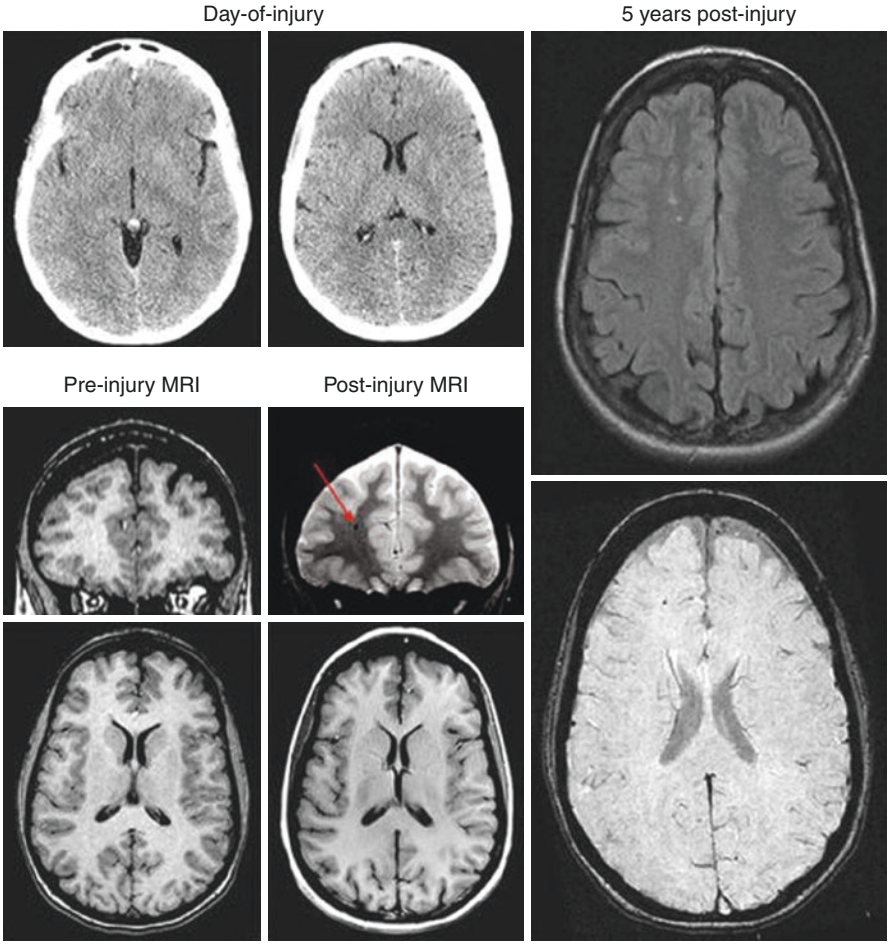

Fig. 8.5 This young adult sustained a significant mTBI in an auto-pedestrian injury where she had positive LOC, but the DOI CT revealed no abnormality. However, as symptoms persisted, this patient was assessed with MRI which revealed hemosiderin and focal white matter hyperintensities. Interestingly, this patient had participated as a research subject prior to the injury, confirming no prior brain abnormalities, as shown in the preinjury MRI, although only a T1-weighted MRI had been performed

stable over the next 5 years of follow-up and represent common neuroimaging sequelae associated with mTBI. The follow-up scans objectively document the damage from the mTBI and also demonstrate the insensitivity of CT in detecting some microhemorrhages and WM pathology associated with mild injury as well as other pathologies that undoubtedly, given the MRI findings, were present on the DOI but below the threshold for CT detection. With regard to the timeline of symptom onset, what is of particular interest as demonstrated in this case is that it took several days for the full effects of the mTBI to be manifested and weeks to diminish

but chronic deficits remained as would be expected given the MRI findings, consistent with shear damage within the frontal lobes.

Although the positive LOC in mTBI is abrupt and an obvious indicator of TBI, by definition for mTBI it has to be brief and transient or, otherwise, the injury would no longer be considered "mild." LOC is also not a criterion for sustaining mTBI [31]. The evolution of symptoms/problems associated with the initial injury, regardless of whether there is alteration in level of consciousness, likely has much to do with complex cellular responses to the mechanical deformation of brain parenchyma following injury [32, 33]. Indeed, the fact that there may be an evolution of the pathophysiology of mTBI subsequent to the initial injury is well established [31, 34], as reviewed in the previous edition of *Concussion in Athletics*. Although mTBI is initiated by an event involving traumatic deformation of neural tissue, the event does not induce a singular, universal pathological event, but initiates the most complex array of structural and physiological changes in brain parenchyma. If the biomechanical deformation is minimal, only transient disruption in neuron integrity may occur [3, 26, 35]. This is depicted in the schematic presented in Fig. 8.6 [36], based on cultured neurons, that have been mechanically stretched to mimic injury, from minimal and transient to maximal with permanent damage. This illustration provides a nice heuristic, albeit simplistic, to visualize

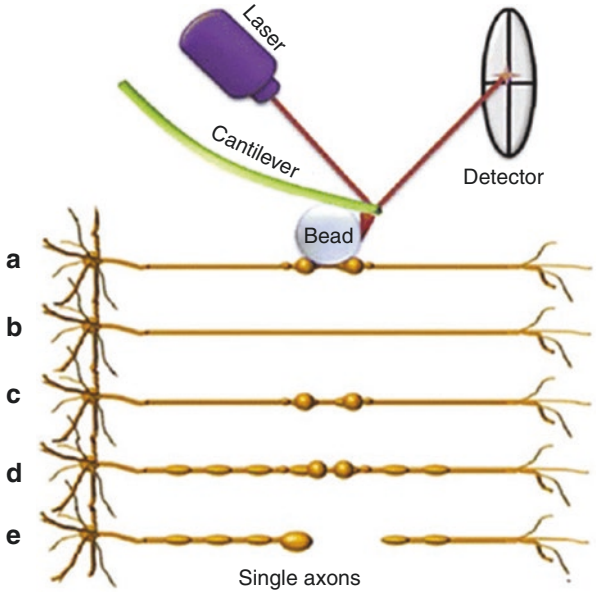

Fig. 8.6 This illustration depicts various potential axonal outcomes following stretch injury in an in vitro TBI model. (**a**) Shows stretch sufficient to create axon beading, which may have transient effect if minimal enough and as shown in (**b**) where axon morphology returns to baseline with no identifiable structural abnormality. However, initial beading may progress, as shown in (**c**) and (**d**), resulting in axon discontinuity and degeneration as shown in (**e**). (From Magdesian et al. [36]; used with permission)

what may occur following mTBI. Note, in this heuristic, transient injury may not lead to structural damage. In such a scenario, the injury did not reach a severity threshold where reparative influences could not overcome the initial cascade of potentially permanent damaging effects from the traumatic pathophysiological events. However, with more significant perturbation, the deformation may begin a process that results in irregular axon morphology and synaptic discontinuities to complete axonal degradation.

In Fig. 8.6, if structural neuroimaging is performed at point "b" in the illustration, there may be no structural neuroimaging counterpoint to show the injury or the damage that was initially induced. As such, the timing issue when neuroimaging is performed also relates to the complexity of what attends even a mild injury. Since when and what type of pathology is expressed further complicates what may be detected with neuroimaging techniques at any point in time postinjury, this underscores the importance of multimodality neuroimaging. For example, the pathobiological complexity mTBI based on severity and time postinjury can be readily demonstrated via in vitro models of stretch injury [37–39]. In their rodent model, Morrison et al. [38] used cultured cells, and then subjected them to stretch injury of different severity. Dependent on the severity of stretch and time postinjury, differences in damage occurred. For some cells, damage may be immediately sufficient to cause cell death, whereas other cells may just be rendered physiologically unstable but with the potential to return to baseline, whereas others progressively die or survive. Those who survive do so with the potential for altered physiological and structural properties.

Churchill and colleagues [40] (see also [41–43]) demonstrate this fluctuating change by plotting how dynamic influences in structural and functional pathologies may emerge in neuroimaging over time as depicted in Fig. 8.7. A take-home message from this illustration, as stated by Churchill et al. is that "Different physiologic aspects of the brain have different concussive recovery times, which can be observed by using MRI." How and when the physiological changes occur also influences when structural changes might be observed.

If a concussive injury is to be but a transient perturbation of physiological integrity, a large array of cellular functions must overtime return to homeostatic baseline. Translating this into what may occur in human mTBI, Fig. 8.8 shows how cognitive and neuroimaging findings change over time in mTBI during the first 8 days [44]. All of these mTBI patients had experienced an "uncomplicated" mTBI, meaning that no abnormalities were identified in the DOI CT scan, almost all with a GCS of 15 and all owing to the result of some type of motor vehicle accident. All subjects were assessed within 2 days of injury, and serially at days 3–4, 5–6, and 7–8 postinjury. Alternate forms of the Hopkins Verbal Learning Test-Recall (HVLT-R) were administered at each time point and, as can be seen in Fig. 8.8, memory performance typically dipped between days 3 and 6, suggesting the confluence of primary and secondary effects from mTBI reaching their apex at this point. Interestingly, these subjects were also assessed at each time point with MRI and diffusion tensor imaging (DTI), where the fractional anisotropy (FA) measurement was obtained on

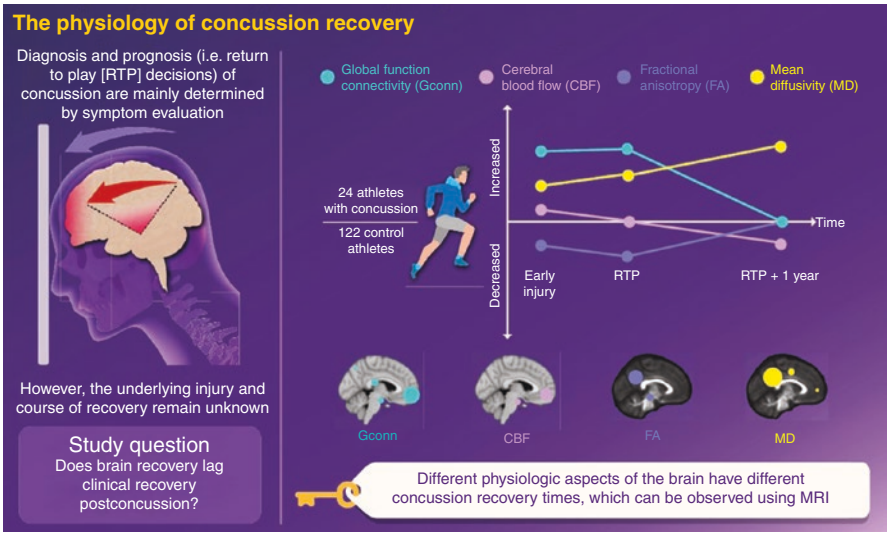

Fig. 8.7 This illustration is from Churchill et al. [40] and illustrates how different neuroimaging modalities detect changes over time in mild TBI. (Reproduced with permission from Neurology)

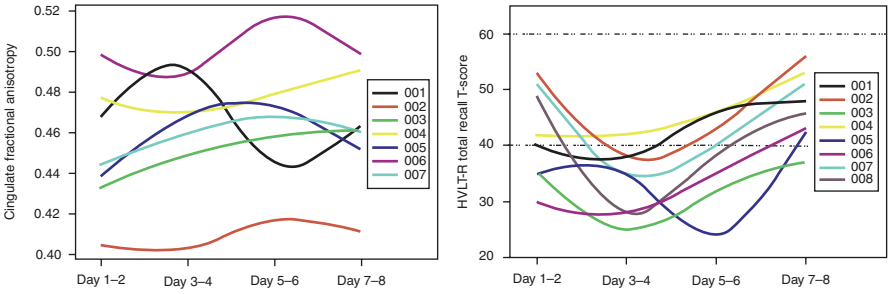

Fig. 8.8 Fractional anisotropy (FA) serial plots over the first 8 days postinjury for seven mTBI patients plotted with corresponding memory performance on the Hopkins Verbal Learning Test-Recall (HVLT-R) performed on the same day as the neuroimaging (note one patient did not have the serial neuroimaging performed). Note the fluctuation in FA, but also the general reduction in memory performance between days 3–4 and 7–8. (From Wilde et al. [44]; used with permission)

each occasion. As plotted in Fig. 8.8, FA exhibited variable fluctuations within each individual as did memory function over the first 8 days postinjury. In mTBI, acute increases in FA may reflect neuroinflammation [3] and, as seen in Fig. 8.8, several mTBI patients showed FA peaks between days 3–4 and 7–8. Decrease in FA may reflect axon damage but without preinjury neuroimaging to know precisely where each individual's FA baseline made it difficult to fully interpret these findings. However, from a memory performance perspective, almost all showed a decrease after day 1–2, with PCS symptoms reaching their peak around day 3. This does

suggest that the variability in FA during this acute/subacute time frame may reflect instability of WM microstructure associated with the injury.

Computed Tomography in mTBI

CT imaging is especially rapid and, with contemporary technology, can be completed within seconds to minutes in the acutely injured individual. Since it uses X-ray beam technology, it is not influenced by paramagnetic objects like those which occur with MRI and, therefore, life support and other medical assist devices do not necessarily interfere with image acquisition or preclude its use. Likewise, metallic fragments from injury that may be paramagnetic can be imaged without concern about displacement by the strong magnetic fields generated by MRI, although image distortion occurs. Excellent contrast between bone and brain parenchyma can be achieved with CT, where CT clearly has the advantage over MRI in demonstrating the presence and location of skull fractures, common sequelae with head injury. CT also provides methods for examining cerebrovascular integrity, blood flow, and inflammation in TBI [45].

In mTBI, the commonly identified abnormalities that can be visualized using CT imaging are surface contusions typically at the brain-skull interface, petechial hemorrhages, and/or localized edema (see Fig. 8.1). The presence of petechial hemorrhage in TBI is considered a marker of DAI [3], two examples of which are shown in Fig. 8.9. Skull fracture is also readily identifiable with CT and must be considered as an indicator of potential brain injury because the distinct forces necessary to fracture bone are certainly sufficient to injure brain parenchyma. Often because of

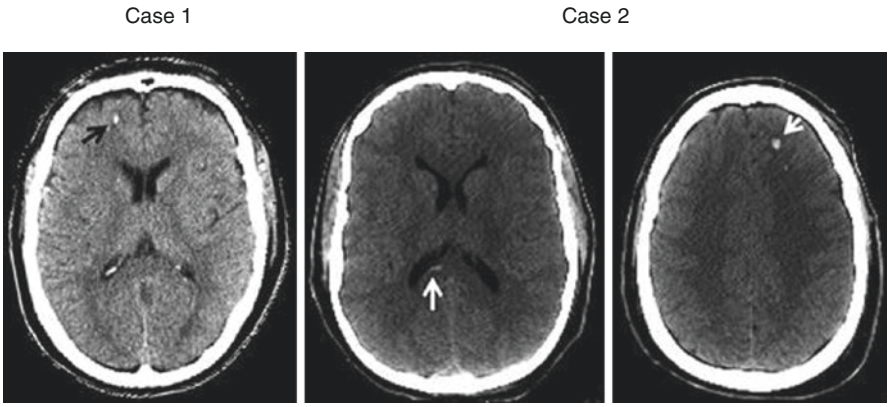

Fig. 8.9 CT appearance of petechial hemorrhage in two separate cases. Note the proximity of the lesion within the white matter but at the border of where the gray boundary is located. Both cases were adults and involved high-speed motor vehicle accidents. Note the *black arrow* in *Case 1* and the *top white arrow* in *Case 2* point to the hemorrhage which occurs right at the gray-white junction. In *Case 2* there is a contrecoup hemorrhagic lesion in the posterior corpus callosum, *bottom arrow*

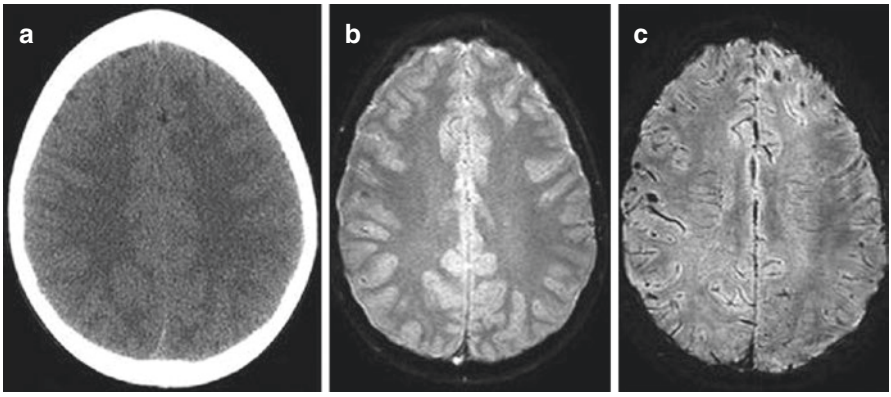

Fig. 8.10 The insensitivity of CT (**a**) and conventional gradient recalled echo (GRE, **b**) sequences to detect petechial hemorrhage are shown. The CT scan was interpreted to be within normal limits with no hemorrhage identified yet this individual agreed to participate in a research study and, therefore, was scanned with MRI procedures including susceptibility weighted imaging (SWI) as shown in (**c**) and magnetization transfer imaging (MTI, not shown), both show frontal abnormality and residual hemorrhage. (From Bigler [60]; used with permission)

the limited resolution of CT, even in the presence of some type of skull fracture in an individual with mTBI, parenchyma may appear normal on CT. Of course, just because neural tissue may appear "normal" does not mean normal microstructure and function because that is beyond the scope of what CT may detect [3, 11].

When an abnormality is present on the DOI CT, as stated earlier, criteria for the classification of "complicated mild TBI" are made. However, given contemporary advances that identify mTBI abnormalities that simply are not detected by CT imaging, this classification is mostly meaningless. Figure 8.5 demonstrated this point and another case is shown in Fig. 8.10. The presence of hemosiderin deposition is presumed to be the best marker for the existence of traumatic shear injury [3]. Currently, the superior MRI method for detecting hemorrhagic shear lesions in mTBI is susceptibility weighted imaging (SWI).

CT imaging readily identifies more serious acute injuries or evolving TBI pathologies that require neurosurgical intervention and is of critical importance in the initial triage and medical management of TBI, including mTBI [18, 46]. With that being said, however, it is of limited utility in mTBI [19].

Visible Macroscopic Abnormalities

To best understand what information may be gathered from MRI in TBI, it is important to appreciate that the abnormalities are, in part, as previously mentioned, time dependent and differ by primary as well as secondary injury effects. Bigler and Maxwell [47, 48] have outlined a time frame depicting the potential pathological changes that occur as presented in the schematic shown in Fig. 8.11, which depicts

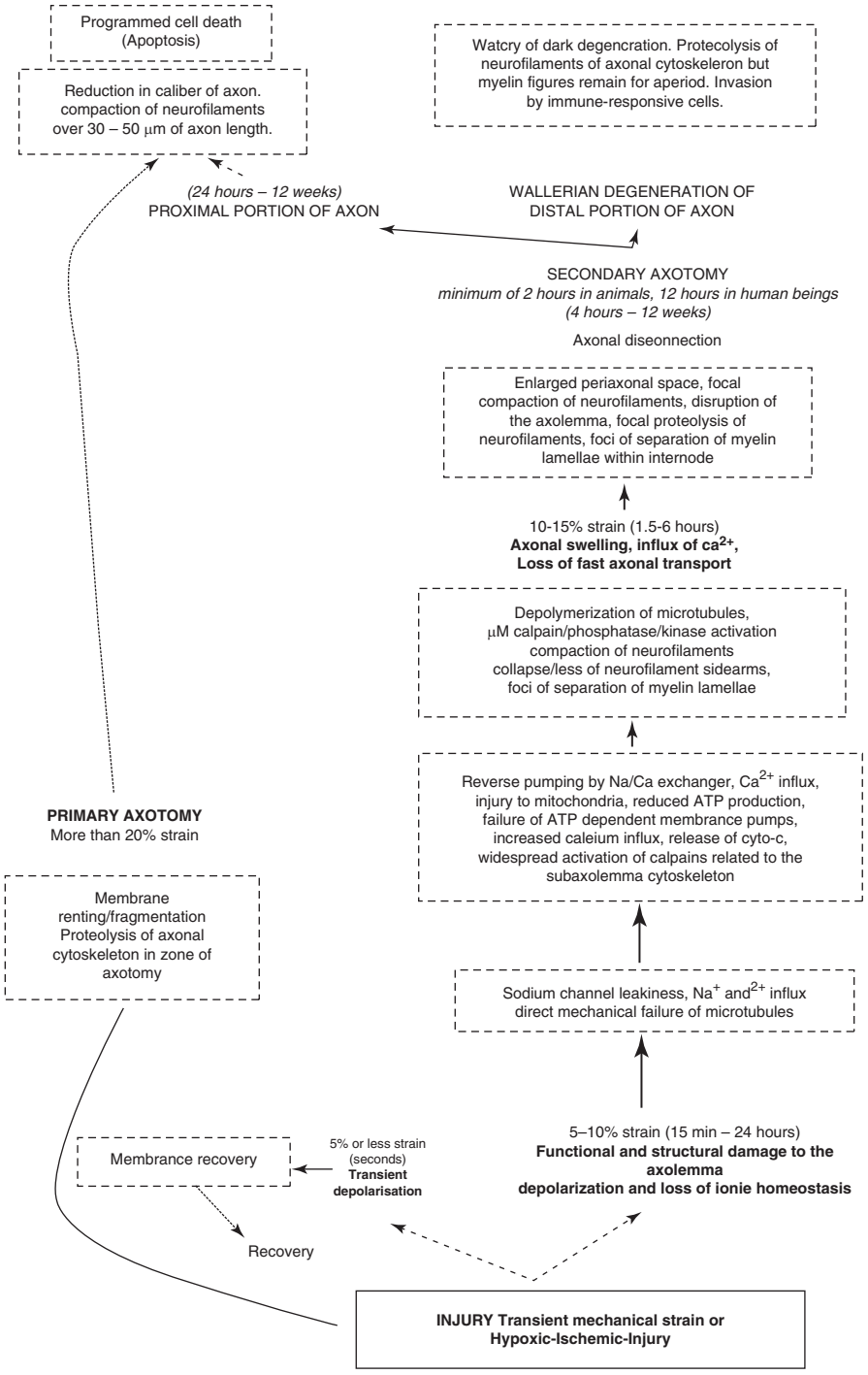

Fig. 8.11 Schematic overview of current thinking with regard to axonal injury in human DAI and animal diffuse traumatic brain injury. (Modified from Biasca and Maxwell [35] and from Bigler and Maxwell [47]; used with permission)

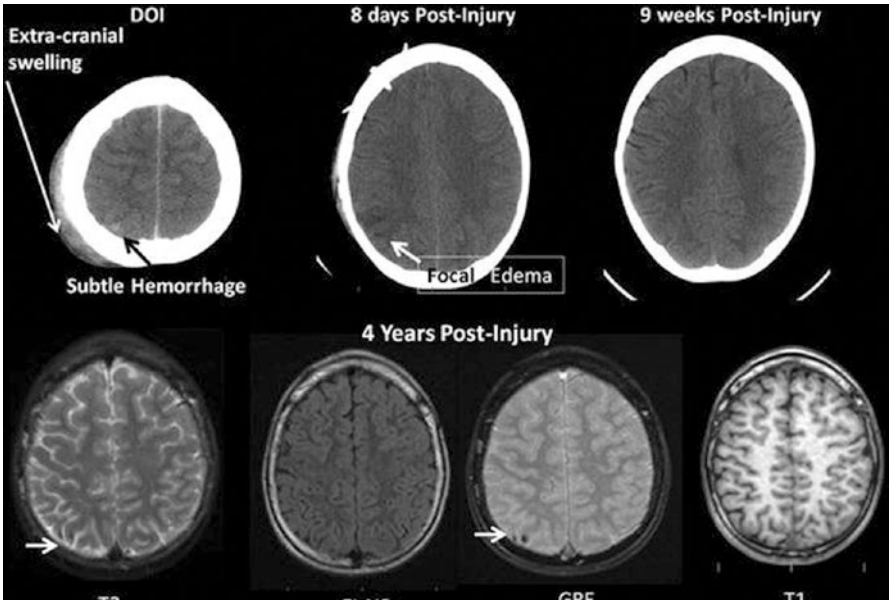

Fig. 8.12 Starting with the DOI CT scans, various lesion types are identified and using the DOI scan as baseline, changes from DOI to chronic state may be shown. The "lesion" starts off as a subtle subarachnoid hemorrhage, but by 8 days postinjury, it is seen as edema which appears to resolve by 9 weeks postinjury. However, with follow-up MRI, subtle hemosiderin deposition is identified

how visibly detectable lesions change over time. Characteristic primary and secondary pathologies can be readily defined when sequential imaging is performed, typically a combination of CT and MRI, as shown in Fig. 8.12.

In Fig. 8.12, the acute CT findings depict the faint appearance of blood, mostly likely indicative of a traumatic subarachnoid hemorrhage. The presence of hemorrhage in TBI, whether detected by CT or MRI, is commonly considered the best indicator of intracranial traumatic shear forces sufficient to produce traumatic axonal injury (TAI) [47, 48], since there was obvious biomechanical force to induce hemorrhage. However, even with the best of resolution that CT imaging provides, precise detection and localization of significant pathology is limited as demonstrated in Fig. 8.12. By 8 days postinjury, edema is identified, but the hemorrhage has basically resolved where phagocytosis has removed degraded blood by-products. By 2 months postinjury, CT imaging demonstrates what appears to be resolution. However, when scanned 4 years later with MRI, hemosiderin deposition is distinctly apparent not in the subarachnoid space, but within brain parenchyma. Imaging of the gyri where the hemorrhage was identified also distinctly demonstrates signal abnormality beyond the hemosiderin foci. When viewed with MRI and knowing the sequence of events, the initial impact forces in this region likely sheared both blood vessels and neural tissue, resulting in DAI and focal WM changes. However, the DOI CT mostly depicts subarachnoid hemorrhage, with little

indication of underlying WM damage. Only through sequential imaging does the true clinical significance of this injury become apparent.

Combining information from Figs. 8.11 and 8.12, the primary and secondary effects of TBI can be inferred. At the point of impact, the primary injury occurs, and given the follow-up MRI findings there likely was traumatic shear injury resulting in primary axotomy. However, considerable secondary injury also likely occurred because of the edema, as well as vascular injury, and whatever local pathologic, metabolic, and neurotransmitter derangements and aberrations that occurred. Sheared blood vessels can no longer provide oxygenated blood to the neuropil resulting in additional neural tissue (both neurons and glial cells) compromise, degradation, and potential death. This becomes the source for focal atrophy. Neuronal degeneration ensues which cannot be detected by CT imaging but is revealed by MRI. This potential sequence of events and its adverse influence on the axon is depicted in Fig. 8.13 [35, 49].

Empirically Derived Quantitative MR Abnormalities

The common images generated from MR technology, like those shown in the various figures up to this point have all been generated by MR display metrics that form the basis for the image presentation. However, these quantitative MR metrics permit

Fig. 8.13 Evolving pathophysiology of traumatic injury in myelinated axons. In this figure, the author's attempts, in an abbreviated fashion, to illustrate some of the key events believed to be involved in the pathobiology of traumatic axonal injury and, thereby, identify potential therapeutic targets. Although framed in the view of primary nodal involvement (**a**), this focus does not preclude comparable change ongoing in other regions of the axon. Panels **b** and **c** show normal axonal detail including the paranodal loops and the presence of intraaxonal mitochondria, microtubules, and neurofilaments, together with the presence of multiple axolemmal channels localized primarily to the nodal domain. Mild-to-moderate traumatic brain injury in panel **d** is observed to involve a mechanical dysregulation of the voltage-sensitive sodium channels, which contribute to increased calcium influx via reversal of the sodium calcium exchanger and the opening of voltage-gated calcium channels. This also impacts on the proteolysis of sodium channel inactivation that contributes further to local calcium dysregulation. Microtubular loss, neurofilament impaction, and local mitochondrial damage can follow, which, if unabated, collectively alters/impairs axonal transport illustrated in panel **e**. Alternatively, if these abnormalities do not progress, recovery is possible (**f**). When progressive, these events not only impair axonal transport but also lead to rapid intraaxonal change in the paranodal and perhaps internodal domains that elicit the collapse of the axolemma and its overlying myelin sheath to result in lobulated and disconnected axonal segments (**g**) that, over the next 15 min–2 h, fully detach (**h**). The proximal axonal segment in continuity with the cell body of origin now continues to swell from the delivery of vesicles and organelles via anterograde transport while the downstream fiber undergoes Wallerian change (**i**). Finally, with the most severe forms of injury, the above identified calcium-mediated destructive cascades are further augmented by the poration of the axolemma, again primarily at the nodal region (**j**). The resulting calcium surge, together with potential local microtubular damage and disassembly, pose catastrophic intraaxonal change that converts anterograde into retrograde axonal transport, precluding continued axonal swelling, while the distal axonal segment fragments and disconnects (**k**), with Wallerian degeneration ensuing downstream (**l**). (From Smith et al. [49]; used with permission)

analyses separate from just the anatomical image display. For example, Fig. 8.14 shows the appearance of a DTI MR sequence with its associated color map. Two common metrics derived from DTI are referred to as fractional anisotropy or FA and apparent diffusion coefficient or ADC. Figure 8.14 provides a DTI schematic depicting the relationship of FA and ADC to axon integrity and what happens with axon

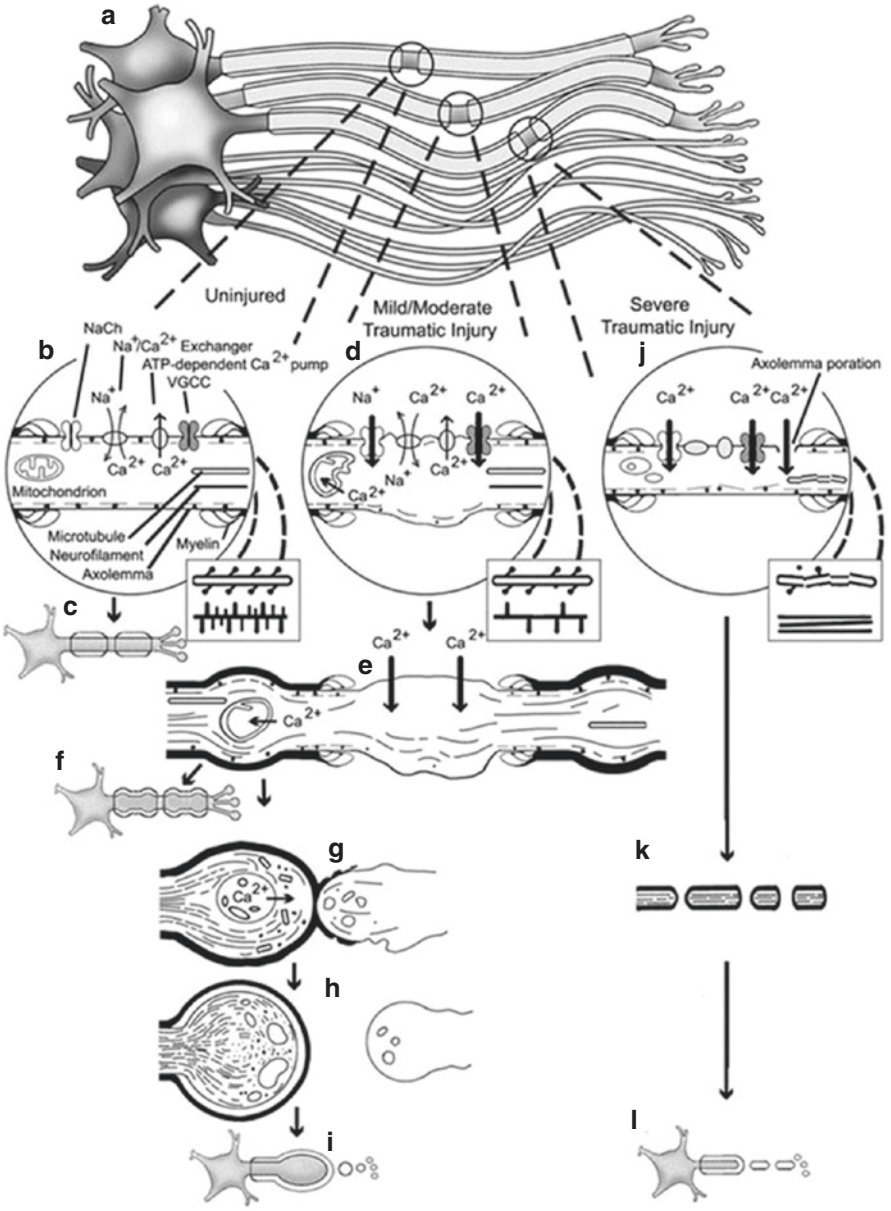

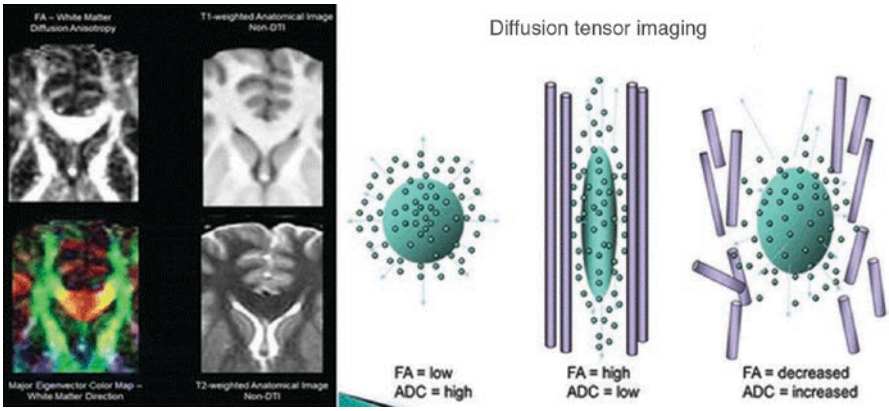

Fig. 8.14 [*Top*] The images on the *upper left* show the DTI acquisition image and the DTI color map (*middle left*) in comparison to the conventional T1 and T2. The cartoon on the *right* depicts the relationship of fractional anisotropy (FA) with the apparent diffusion coefficient (ADC) showing how normal conformity of membrane anatomy constrains water diffusion; however, if membrane dissolution occurs in any fashion, such as from TBI, water is freer to move and with lack of constraint, FA elevates and ADC declines. [*Bottom*] Results of voxel-wise meta-analysis findings of where DTI differences are most likely to occur based on the review by Hunter and Lubin [50]. Fractional anisotropy (FA) in those with TBI subjects demonstrated one cluster of high FA (red) in the right superior longitudinal fasciculus and seven clusters of low FA (blue), the largest two located in the corpus callosum

damage. These DTI metrics assess the microstructure of WM and are based on the characteristics of how myelin sheaths and cell membranes of WM tracts affect the movement of water molecules. Healthy axonal membranes constrain the free movement and direction of movement of water. Consequently, water molecules tend to move faster in parallel to nerve fibers rather than perpendicular to them. This characteristic, which is referred to as anisotropic diffusion and is measured by FA, is determined by the thickness of the myelin sheath and of the axons. FA ranges from 0 to 1, where 0 represents maximal isotropic diffusion (e.g., free diffusion in perfect sphere) and 1 represents maximal anisotropic diffusion, that is, diffusion in one direction (e.g., a long cylinder of minimal diameter). Diffusion anisotropy varies across WM regions, putatively reflecting differences in fiber myelination, fiber diameter, and directionality.

The aggregate fiber tracts of an entire brain can be derived from DTI, as shown in Fig. 8.15. In TBI, DTI may demonstrate a loss of fiber tract integrity, reflected as a thinning out of the number of aggregate tracts. This is also demonstrated in Fig. 8.15, where a patient with TBI is compared to a similar aged individual with typical development. The loss of aggregate tracts in the TBI whole-brain network analysis demonstrates an overall reduction in WM connectivity. DTI methods provide various techniques to view the pathological effects of TBI within the context of WM network connectivity.

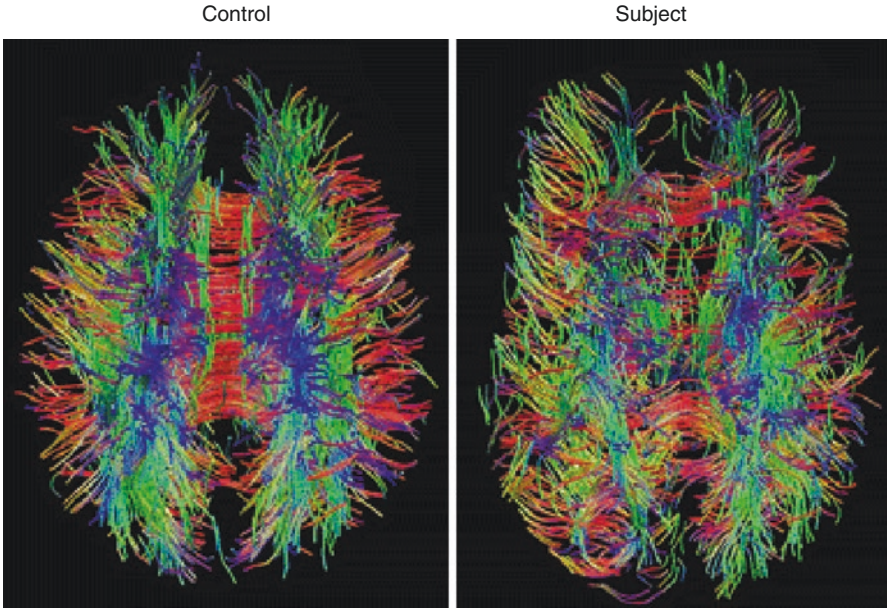

Fig. 8.15 DTI-derived aggregate tracts of the brain can be visualized where in a healthy adult, the dorsal view of the control participant on the left depicts the dense organization of fiber tracts where green streamlines show tract orientation (red/orange = laterally projecting tracts, blue = vertically orientated tracts and green = anterior-posterior projections). In the TBI subject on the right who had sustained a severe TBI, thinning of the tracts is visibly obvious implicating widespread loss of white matter integrity

When DTI metrics are applied to milder injuries, the dramatic changes as visualized in Fig. 8.15 are typically not observed but at a group level, a variety of characteristic changes in WM integrity may be detected. For example, returning to Fig. 8.14, the illustration from Hunter and Lubin [50] summarizes DTI findings involving an mTBI review and meta-analysis of quantitative DTI findings, where the most overlapping abnormalities have been reported. As shown in Fig. 8.14 (bottom), the most common FA changes are consistently observed in mild TBI that occurs within the corpus callosum.

Trauma-induced edematous reactions in the brain compress parenchyma, which in turn, may influence water diffusion potentially detected by DTI. Using the FA metric, increases in FA beyond some normal baseline may signify neuroinflammation, whereas low FA may occur when axon degradation and membrane abnormalities increase water diffusion or when actual degeneration has occurred, which increases extracellular water [3]. Since TBI may induce dynamic changes over time, differences in FA over acute, subacute, and chronic time frames postinjury may differ as well. When axons degenerate, the increased space frees extracellular water, resulting in lower FA. Thus, in mTBI, low FA may reflect WM degeneration with increased FA beyond normative baseline, and may indicate neuroinflammation [51, 52].

Heterogeneity Visible mTBI Lesions

Bigler et al. [8] examined a sample of 41 children with complicated mTBI. When assessed with MRI at least 6 months postinjury, regardless of whether the residual lesion was an area of focal encephalomalacia, hemosiderin deposit, or WM hyperintensity, *none* of the lesions perfectly overlapped, although the majority were distributed within the frontal and temporal lobes. Just from the randomness of the lesions, this would indicate that each mTBI produced its own unique injury and with unique injury this would indicate the likelihood that mTBI sequelae would likely be rather idiosyncratic to the individual as well.

Cellular Basis of mTBI Neuropathology

Based on the position statement by the International and Interagency Initiative toward Common Data Elements for Research on Traumatic Brain Injury and Psychological Health, the definition of traumatic brain injury is "… an alteration in brain function, or other evidence of brain pathology, caused by an external force [31]." External force induces brain injury via deformation of neural tissue that surpasses tolerance limits for normal displacement or strain that accompanies movement such as jumping, rapid turning of the head, and simple bumps to the head. So, at the most fundamental level of injury, cellular deformation disrupts anatomy and physiology sufficient to at least transiently impair function when the threshold for mTBI has been reached.

Too often, neural cells are viewed schematically as an artist's rendition of what a neural cell looks like, such as that shown in Fig. 8.16, but artistic schematics detract from the true complexity and delicate nature of what really constitutes neural tissue. For example, Fig. 8.16 depicts two cortical pyramidal cells identified in the rat cerebral cortex based on their physiological response and their appearance via electron microscopy. Note how small these structures are and that these views are merely two dimensional of a three-dimensional structure and note that the axon is but a few microns in thickness. Additionally, note the numerous dendritic spines and how the axon intertwines with the spines. Understanding this delicate balance of what generates brain parenchyma makes it easier to understand why deformation of neural tissue may be injurious.

As the definition implies, TBI occurs from some external force, which in turn must deform brain parenchyma such that a sufficient distortion of the typical shape of cellular tissue no longer lines up and/or connects as it should. Returning to Fig. 8.16, note again the complex intertwining of dendritic spines with axon segments where any misalignment would likely affect synaptic integrity. Likewise, if the axon membrane is disrupted, membrane permeability will directly impact neuronal function and propagation of axon potentials. Only one axon segment needs to be affected to disrupt neural transmission for the entire axon. A variety of finite elements and various methods for recreating the motion that displaces brain parenchyma that results in concussive injury have been performed, mostly using sports

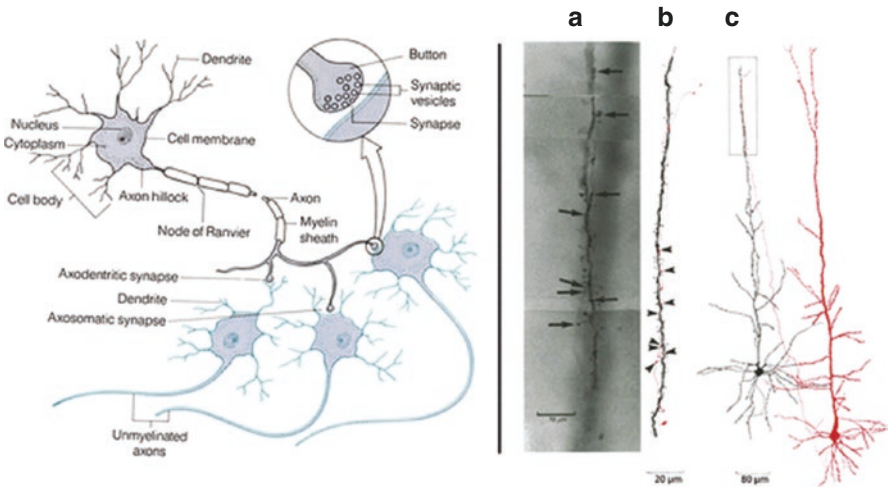

Fig. 8.16 (*Left*) The schematic of a neuron shows a hypothetical neuron with what appears to be a bulky, sturdy axon protruding from the cell body and interfacing with other neurons. However, the reality is something quite different. (From Pinel [61]; used with permission). (*Right*) Two cortical cells in a rat cortex that have been isolated. Note the micron level of the axon—it is infinitesimally small. Note also how the single axon intertwines the dendrite and the dendritic spines as highlighted in the photomicrograph. When thinking about TBI, one must view the potential neuropathological effects at this microscopic level. (From Deuchars et al. [62]; used with permission)

concussion models. For example, Viano et al. [53] showed on average in the typical sports-related concussion that the brain displaces between 4 and 8 mm in regions like the corpus callosum, midbrain, medial temporal lobe, and fornix. Viewing Fig. 8.16 from the perspective of this amount of deformation, noting that the photomicrograph depicts an axon that is about 0.1 mm in length, would reflect a massive distortion of neurons of this size.

Blood vessels are just as delicate as neural tissue, especially at the capillary level. Each neuron is dependent on receiving a continuous source of glucose and oxygen with the smallest capillaries large enough for just a single red blood cell to traverse the capillary to deliver its oxygen and glucose [47, 48]. As such, blood vessels are just as susceptible to the shear–strain biomechanics of head injury as are neurons [54].

Deformation Biomechanics and the Most Vulnerable Areas for Brain Injury

From the above discussion, all deformation in mTBI must be viewed at the cellular level, but biomechanical schematics are typically presented at the whole brain level. Ropper and Gorson [55] provided a schematic of where the greatest deformations have been modeled in mTBI and this is provided in Fig. 8.17. This illustration clearly depicts the known frontotemporal regions for cortical surface compression, but also WM tracts of the upper brainstem corpus callosum and cingulum. In mTBI,

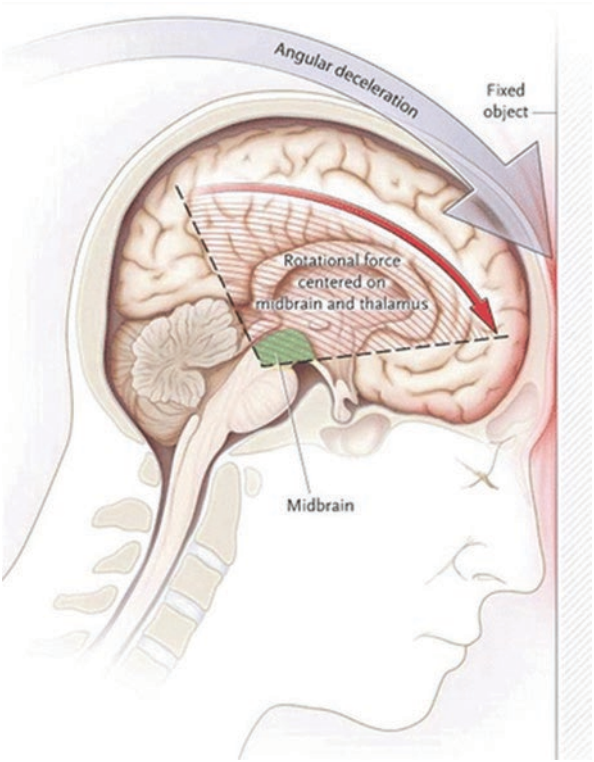

Fig. 8.17 The mechanism of concussion is outlined in this illustration. Biomechanical investigations dating back to the beginning of the twentieth century suggest that concussion results from a rotational motion of the cerebral hemispheres in the anterior-posterior plane, around the fulcrum of the fixed-in-place upper brain stem. If the neck is restrained, concussion is difficult to produce. Concussions as portrayed in movies and cartoons, in which the back of the head is struck with a blunt object and no motion is transferred to the brain, are implausible. The modern view is that there is disruption of the electrophysiological and subcellular activities of the neurons of the reticular activating system that are situated in the midbrain and diencephalic region, where the maximal rotational forces are exerted. Alternative mechanisms for concussive LOC, such as self-limited cortical seizures or a sudden increase in intracranial pressure, have also been proposed, but with limited supporting evidence. An animated version of this figure is available with the full text of the article at www.nejm.org. (From Ropper and Gorson [55]; used with permission)

as already mentioned by definition of what constitutes a TBI, the WM abnormalities at the brainstem level could not represent major pathology because LOC must be brief to meet mTBI criteria. Likewise, alteration in mental status that would result in prolonged posttraumatic amnesia would also disqualify someone for mTBI classification. So while subtle brainstem pathology may persist in the mTBI patient, as Heitger et al. [56] have shown, as well as frontotemporal pathology, as numerous investigators have shown, major pathologies at these levels are unlikely because if major pathology persisted in these regions during the acute phase, the individual likely would not meet criteria for mTBI. Nonetheless, the one that is depicted in

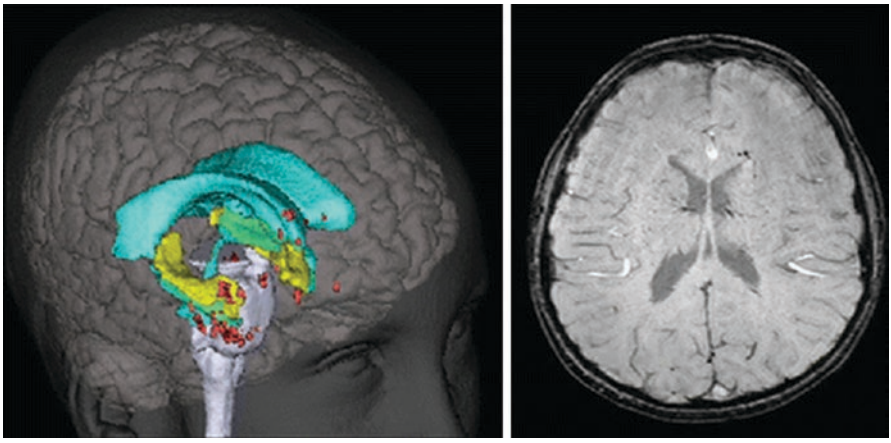

Fig. 8.18 This preadolescent child sustained an mTBI in a ski accident. When symptoms persisted, MRI demonstrated multiple regions of hemosiderin deposition. Note the frontotemporal distribution and location of hemosiderin in the forceps minor region of the corpus callosum on the susceptibility weighted image on the *right*. In the three-dimensional image, the ventricle is shown in aquamarine to provide landmark points with the *red* signifying where hemosiderin was identified, and the *yellow* indicates the hippocampus

Fig. 8.17 from Ropper and Gorson provides a wonderful heuristic for where likely changes in mTBI will be observed in neuroimaging studies.

For example, Fig. 8.18 is from a child with mTBI from a skiing accident who sustained an mTBI. When symptoms persisted, this child, who had a negative DOI CT, was scanned with MRI. The follow-up MRI revealed hemosiderin deposition in frontotemporal areas and anterior corpus callosum, as would be predicted from the schematic in Fig. 8.17. Likewise, note from Fig. 8.14 that the corpus callosum is a common area of DTI defined WM pathology from mTBI.

Volumetry Findings in mTBI

As shown in Fig. 8.17, if atrophic changes associated with mTBI were to occur, they would most likely be found within those regions associated with the greatest likelihood for shear/strain and deformation injury. Indeed, several studies that have prospectively examined mTBI subjects have demonstrated this regional atrophy [3, 57, 58]. For example, Zhou et al. [59] demonstrated that by establishing a baseline in mTBI patients within the acute to early subacute time frame that when assessed with various volumetric techniques 1 year later that significant volume loss was observed in the anterior cingulum, cingulate gyrus, and scattered regions within the frontal lobes. Interestingly, they observed volume loss in the cuneus and precuneus regions as well. The volume loss with the cuneus and precuneus, posterior brain regions, may actually be the result of Wallerian degeneration from the more focal frontal loss disrupting long-coursing frontoparietal connections particularly

vulnerable to stretching and shearing effects [3]. Sussman and da Costa [58] applied volumetric analyses to assess cortical morphometry in those with mTBI and concluding the following: "… a single concussive episode induces measurable changes in brain structure manifesting as diffuse and local patterns of altered neuromorphometry (p. 650)."

Conclusion

Structural neuroimaging provides a variety of methods to detect underlying neuropathology that results from mTBI. The most common visible abnormalities are in the form of focal encephalomalacia, hemosiderin deposition, and/or WM hyperintensity. A variety of quantitative MRI methods have demonstrated techniques for the detection of underlying pathology associated with mTBI, which differ depending on the time postinjury that the scan is performed.

References

1. Fidan E, et al. Metabolic and structural imaging at 7 tesla after repetitive mild traumatic brain injury in immature rats. ASN Neuro. 2018;10:1759091418770543.
2. Schweser F, et al. Visualization of thalamic calcium influx with quantitative susceptibility mapping as a potential imaging biomarker for repeated mild traumatic brain injury. NeuroImage. 2019;200:250–8.
3. Victoroff J, Bigler ED. Concussion and traumatic encephalopathy. New York: Cambridge University Press; 2019.
4. Mayer AR, et al. Radiologic common data elements rates in pediatric mild traumatic brain injury. Neurology. 2020;94(3):e241–53.
5. Bigler ED. Systems biology, neuroimaging, neuropsychology, neuroconnectivity and traumatic brain injury. Front Syst Neurosci. 2016;10:55.
6. Bigler ED. Structural neuroimaging in sport-related concussion. Int J Psychophysiol. 2018;132(Pt A):105–23.
7. Teasdale G, Knill-Jones R, van der Sande J. Observer variability in assessing impaired consciousness and coma. J Neurol Neurosurg Psychiatry. 1978;41(7):603–10.
8. Bigler ED, et al. Heterogeneity of brain lesions in pediatric traumatic brain injury. Neuropsychology. 2013;27(4):438–51.
9. Perez-Polo JR, et al. A rodent model of mild traumatic brain blast injury. J Neurosci Res. 2015;93(4):549–61.
10. Hylin MJ, et al. Behavioral and histopathological alterations resulting from mild fluid percussion injury. J Neurotrauma. 2013;30(9):702–15.
11. Hoogenboom WS, et al. Diffusion tensor imaging of the evolving response to mild traumatic brain injury in rats. J Exp Neurosci. 2019;13:1179069519858627.
12. Raizman R, et al. Traumatic brain injury severity in a network perspective: a diffusion MRI based connectome study. Sci Rep. 2020;10(1):9121.
13. Arnatkeviciute A, Fulcher BD, Fornito A. Uncovering the transcriptional correlates of hub connectivity in neural networks. Front Neural Circuits. 2019;13:47.
14. Sporns O. Structure and function of complex brain networks. Dialogues Clin Neurosci. 2013;15(3):247–62.
15. Bailey SK, et al. Applying a network framework to the neurobiology of reading and dyslexia. J Neurodev Disord. 2018;10(1):37.

16. van den Heuvel MP, Sporns O. Rich-club organization of the human connectome. J Neurosci. 2011;31(44):15775–86.
17. Bigler ED, et al. Structural neuroimaging findings in mild traumatic brain injury. Sports Med Arthrosc Rev. 2016;24(3):e42–52.
18. Douglas DB, et al. Neuroimaging of traumatic brain injury. Med Sci (Basel). 2018;7(1):2.
19. Suri AK, Lipton ML. Neuroimaging of brain trauma in sports. Handb Clin Neurol. 2018;158:205–16.
20. Slobounov S, et al. Concussion in athletics: ongoing clinical and brain imaging research controversies. Brain Imaging Behav. 2012;6(2):224–43.
21. Griauzde J, Srinivasan A. Advanced neuroimaging techniques: basic principles and clinical applications. J Neuroophthalmol. 2018;38(1):101–14.
22. Wilde EA, Hunter JV, Bigler ED. A primer of neuroimaging analysis in neurorehabilitation outcome research. NeuroRehabilitation. 2012;31(3):227–42.
23. Post A, Hoshizaki B, Gilchrist MD. Finite element analysis of the effect of loading curve shape on brain injury predictors. J Biomech. 2012;45(4):679–83.
24. Statler KD, et al. Traumatic brain injury during development reduces minimal clonic seizure thresholds at maturity. Epilepsy Res. 2008;80(2–3):163–70.
25. Smith D, et al. Multi-excitation MR elastography of the brain: wave propagation in anisotropic white matter. J Biomech Eng. 2020;142(7):0710051.
26. Okamoto RJ, et al. Insights into traumatic brain injury from MRI of harmonic brain motion. J Exp Neurosci. 2019;13:1179069519840444.
27. Kraft RH, et al. Combining the finite element method with structural connectome-based analysis for modeling neurotrauma: connectome neurotrauma mechanics. PLoS Comput Biol. 2012;8(8):e1002619.
28. Watanabe R, et al. Research of the relationship of pedestrian injury to collision speed, car-type, impact location and pedestrian sizes using human FE model (THUMS version 4). Stapp Car Crash J. 2012;56:269–321.
29. Prichep LS, et al. Time course of clinical and electrophysiological recovery after sport-related concussion. J Head Trauma Rehabil. 2013;28(4):266–73.
30. Duhaime AC, et al. Spectrum of acute clinical characteristics of diagnosed concussions in college athletes wearing instrumented helmets: clinical article. J Neurosurg. 2012;117(6):1092–9.
31. Menon DK, et al. Position statement: definition of traumatic brain injury. Arch Phys Med Rehabil. 2010;91(11):1637–40.
32. Hammad A, Westacott L, Zaben M. The role of the complement system in traumatic brain injury: a review. J Neuroinflammation. 2018;15(1):24.
33. Stahel PF, Morganti-Kossmann MC, Kossmann T. The role of the complement system in traumatic brain injury. Brain Res Brain Res Rev. 1998;27(3):243–56.
34. Kamins J, et al. What is the physiological time to recovery after concussion? A systematic review. Br J Sports Med. 2017;51(12):935–40.
35. Biasca N, Maxwell WL. Minor traumatic brain injury in sports: a review in order to prevent neurological sequelae. Prog Brain Res. 2007;161:263–91.
36. Magdesian MH, et al. Atomic force microscopy reveals important differences in axonal resistance to injury. Biophys J. 2012;103(3):405–14.
37. Rosas-Hernandez H, et al. Characterization of uniaxial high-speed stretch as an in vitro model of mild traumatic brain injury on the blood-brain barrier. Neurosci Lett. 2018;672:123–9.
38. Morrison B 3rd, et al. An in vitro model of traumatic brain injury utilising two-dimensional stretch of organotypic hippocampal slice cultures. J Neurosci Methods. 2006;150(2):192–201.
39. Dolle JP, et al. Newfound sex differences in axonal structure underlie differential outcomes from in vitro traumatic axonal injury. Exp Neurol. 2018;300:121–34.
40. Churchill NW, et al. Mapping brain recovery after concussion: from acute injury to 1 year after medical clearance. Neurology. 2019;93(21):e1980–92.
41. Churchill NW, et al. Scale-free functional brain dynamics during recovery from sport-related concussion. Hum Brain Mapp. 2020;41(10):2567–82.

42. Di Battista AP, et al. The relationship between symptom burden and systemic inflammation differs between male and female athletes following concussion. BMC Immunol. 2020;21(1):11.
43. Churchill NW, et al. Baseline vs. cross-sectional MRI of concussion: distinct brain patterns in white matter and cerebral blood flow. Sci Rep. 2020;10(1):1643.
44. Wilde EA, et al. Serial measurement of memory and diffusion tensor imaging changes within the first week following uncomplicated mild traumatic brain injury. Brain Imaging Behav. 2012;6(2):319–28.
45. Creeden S, et al. Interobserver agreement for the computed tomography severity grading scales for acute traumatic brain injury. J Neurotrauma. 2020;37(12):1445–51.
46. Bonfante E, Riascos R, Arevalo O. Imaging of chronic concussion. Neuroimaging Clin N Am. 2018;28(1):127–35.
47. Bigler ED, Maxwell WL. Neuropathology of mild traumatic brain injury: relationship to neuroimaging findings. Brain Imaging Behav. 2012;6(2):108–36.
48. Bigler ED, Maxwell WL. Neuroimaging and neuropathology of TBI. NeuroRehabilitation. 2011;28(2):63–74.
49. Smith DH, Hicks R, Povlishock JT. Therapy development for diffuse axonal injury. J Neurotrauma. 2013;30(5):307–23.
50. Hunter LE, et al. Comparing region of interest versus voxel-wise diffusion tensor imaging analytic methods in mild and moderate traumatic brain injury: a systematic review and meta-analysis. J Neurotrauma. 2019;36(8):1222–30.
51. Narayana S, et al. Neuroimaging and neuropsychological studies in sports-related concussions in adolescents: current state and future directions. Front Neurol. 2019;10:538.
52. Schneider DK, et al. Diffusion tensor imaging in athletes sustaining repetitive head impacts: a systematic review of prospective studies. J Neurotrauma. 2019;36(20):2831–49.
53. Viano DC, et al. Concussion in professional football: brain responses by finite element analysis: part 9. Neurosurgery. 2005;57(5):891–916; discussion 891–916.
54. Madri JA. Modeling the neurovascular niche: implications for recovery from CNS injury. J Physiol Pharmacol. 2009;60(Suppl 4):95–104.
55. Ropper AH, Gorson KC. Clinical practice. Concussion. N Engl J Med. 2007;356(2):166–72.
56. Heitger MH, et al. Impaired eye movements in post-concussion syndrome indicate suboptimal brain function beyond the influence of depression, malingering or intellectual ability. Brain. 2009;132(Pt 10):2850–70.
57. Bigler ED. Volumetric MRI findings in mild traumatic brain injury (mTBI) and neuropsychological outcome. Neuropsychol Rev. 2021; https://doi.org/10.1007/s11065-020-09474-0.
58. Sussman D, et al. Concussion induces focal and widespread neuromorphological changes. Neurosci Lett. 2017;650:52–9.
59. Zhou Y, et al. Mild traumatic brain injury: longitudinal regional brain volume changes. Radiology. 2013;267(3):880–90.
60. Bigler ED. Neuropsychology and clinical neuroscience of persistent post-concussive syndrome. J Int Neuropsychol Soc. 2008;14(1):1–22.
61. Pinel JPJ. Biopsychology. Boston: Allyn & Bacon; 1990.
62. Deuchars J, West DC, Thomson AM. Relationships between morphology and physiology of pyramid-pyramid single axon connections in rat neocortex in vitro. J Physiol. 1994;478(3):423–35.